CHEMISTRY
A EUROPEAN JOURNAL

DOI: 10.1002/chem.200501578

Charge-Induced Reversible Rearrangement of Endohedral Fullerenes: Electrochemistry of Tridysprosium Nitride Clusterfullerenes $Dy_3N@C_{2n}$ ($2n = 78$, 80)

Shangfeng Yang,[a] Michal Zalibera,[a, b] Peter Rapta,[a, b] and Lothar Dunsch*[a]

Abstract: The electrochemistry of three new clusterfullerenes $Dy_3N@C_{2n}$ ($2n = 78$, 80), namely two isomers of $Dy_3N@C_{80}$ (I and II) as well as $Dy_3N@C_{78}$ (II), have been studied systematically including their redox-reaction mechanism. The cyclic voltammogram of $Dy_3N@C_{80}$ (I) (I_h) exhibits two electrochemically irreversible but chemically reversible reduction steps and one reversible oxidation step. Such a redox pattern is quite different from that of $Sc_3N@C_{80}$ (I), and this can be understood by considering the difference in the charge transfer from the encaged cluster to the cage. A double-square reaction scheme is proposed to explain the observed redox-reaction behavior, which involves the charge-induced reversible rearrangement of the $Dy_3N@C_{80}$ (I) monoanion. The first oxidation potential of $Dy_3N@C_{80}$ (II) (D_{5h}) has a negative shift of 290 mV relative to that of $Dy_3N@C_{80}$ (I) (I_h), indicating that lowering the molecular symmetry of the clusterfullerene cage results in a prominent increase in the electron-donating property. The first and second reduction potentials of $Dy_3N@C_{78}$ (II) are negatively shifted relative to those of $Dy_3N@C_{80}$ (I, II), pointing to the former's lowered electron-accepting ability. The significant difference in the electrochemical energy gaps of $Dy_3N@C_{80}$ (I), $Dy_3N@C_{80}$ (II), and $Dy_3N@C_{78}$ (II) is consistent with the difference in their optical energy gaps.

Keywords: cyclic voltammetry · electrochemistry · fullerenes · isomers · reaction mechanisms

Introduction

Among endohedral fullerenes,[1,2] the trimetallic nitride endohedral fullerenes (clusterfullerenes), a new class of fullerenes with an encaged trimetallic nitride cluster,[3,4] have been attracting great interest since their discovery in 1999.[5] This is because of the feasibility of tuning the trapped metal atoms in these fullerenes and of stabilizing a large variety of cage sizes including different isomeric structures, in addition to them possessing several distinguishing properties,[3–8] which have been investigated for potential applications such as new contrast agents in magnetic resonance imaging (MRI).[4,9,10]

The electrochemistry associated with the novel electronic and supramolecular structures has been recognized as one of the most intriguing properties of endohedral fullerenes.[11–16] Electrochemical characterization of endohedral fullerenes could provide direct insight into their electronic structure and hence appears rather important. Very recently, cyclic voltammograms of clusterfullerenes $Sc_3N@C_{80}$ (I) and $Tm_3N@C_{80}$ (I) were reported by our group.[17,18] Although both clusterfullerenes exhibited two reduction steps and one oxidation step in *o*-dichlorobenzene (*o*-DCB), the shifts of their first reduction and first oxidation potentials due to a difference in symmetry were revealed, suggesting the significant contribution of the wave functions of the encaged cluster (Sc_3N and Tm_3N) to the frontier orbitals of the electronic structures of the fullerene cage.[17,18] Furthermore, the peak current ratio of their voltammograms was also found to be extremely metal dependent.[18] Given that $Sc_3N@C_{80}$ (I) and $Tm_3N@C_{80}$ (I) exhibit the same molecular symmetry (I_h),[17,18] such a strong metal dependence can only be understood by considering the difference in the charge transfer from the encaged cluster to the cage, which has been recently revealed by high-energy spectroscopic stud-

[a] Dr. S. Yang, M. Zalibera, Dr. P. Rapta, Prof. Dr. L. Dunsch
Group of Electrochemistry and Conducting Polymers
Leibniz-Institute for Solid State and Materials Research (IFW)
Dresden, 01171 Dresden (Germany)
Fax: (+49) 351-4659-811
E-mail: l.dunsch@ifw-dresden.de

[b] M. Zalibera, Dr. P. Rapta
Department of Physical Chemistry
Faculty of Chemical and Food Technology
Slovak University of Technology, Radlinskeho 9
81237 Bratislava (Slovak Republic)

Supporting information for this article is available on the WWW under http://www.chemeurj.org/ or from the author.

Pagination corrected Oct. 17, 2006

ies.[18–21] It appears, therefore, quite important to further address the influence of the metal (encaged cluster) on the electrochemical properties of clusterfullerenes.

It is known that fullerene cage isomers have different oxidation potentials,[22,23] and in light of such a difference, a simple separation of two isomers of $Sc_3N@C_{80}$ ((I, I_h) and (II, D_{5h})) was recently accomplished by Echegoyen et al. on the basis of a selective chemical oxidation.[24] A 270 mV difference in the first electrochemical oxidation potentials of the two isomers was revealed.[24] No electrochemical study of the cage isomers of other clusterfullerenes has been reported so far. In addition, a recent electrochemical study of a series of Yb-based monometallofullerenes demonstrated the effect of the cage size on their electrochemical behavior.[23] Therefore, it also appears important to study the effect of the cage size on the electrochemical behavior of the clusterfullerenes.

We report herein the electrochemistry of three new dysprosium-based clusterfullerenes $Dy_3N@C_{2n}$ ($2n=78$, 80), including two isomers of $Dy_3N@C_{80}$ ((I) and (II)) and $Dy_3N@C_{78}$(II). Cyclic voltammograms of these three clusterfullerenes are analyzed in detail also with respect to their electrochemical energy gap. To explain the observed redox-reaction behavior, a reaction scheme is proposed that includes a charge-induced reversible rearrangement of the $Dy_3N@C_{80}$(I) monoanion. The cyclic voltammogram results of these three clusterfullerenes are compared with those for the other reported clusterfullerenes, and the dependence of the redox behavior, charge distribution, and frontier orbitals of the electronic structure on both the metal (cluster) and the cage symmetry are discussed.

Results and Discussion

Identification of the $Dy_3N@C_{2n}$ clusterfullerenes: The chemical identification and purities of the three studied $Dy_3N@C_{2n}$ ($2n=78$, 80) clusterfullerenes were established by using laser desorption time-of-flight (LD-TOF) mass spectrometry running in both positive- and negative-ion modes in combination with high-performance liquid chromatography (HPLC) analysis.[25] Figure 1 presents the LD-TOF mass spectra of the $Dy_3N@C_{2n}$ ($2n=78$, 80) clusterfullerenes (only positive-ion mode is shown). A closer comparison of the measured isotope distributions for the three $Dy_3N@C_{2n}$ clusterfullerenes with the theoretical calculations revealed a good agreement in all cases, confirming the proposed chemical identities.[25] Accordingly, the purities of $Dy_3N@C_{80}$(I), $Dy_3N@C_{80}$(II), and $Dy_3N@C_{78}$(II) were estimated to be higher than 99, 98, and 99%, respectively,[25] ensuring the reliability of the following electrochemical characterization.

Cyclic voltammogram of $Dy_3N@C_{80}$(I): Shown in Figure 2 is the cyclic voltammogram of $Dy_3N@C_{80}$(I) dissolved in *o*-dichlorobenzene (*o*-DCB) with ferrocene (Fc) added as the internal standard and that of the blank electrolyte solution

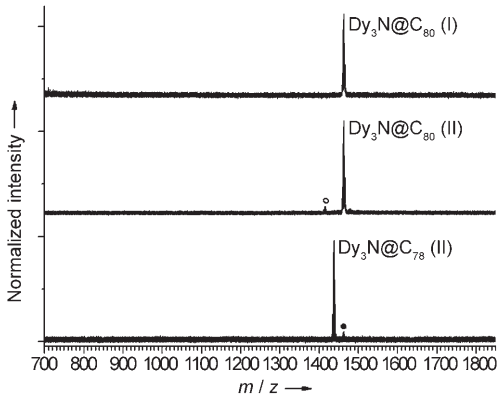

Figure 1. Positive-ion laser desorption time-of-flight (LD-TOF) mass spectra of the studied $Dy_3N@C_{2n}$ clusterfullerenes. The open and filled circles represent the nonseparable minor impurities of $Dy_3N@C_{76}$ and $Dy_3N@C_{80}$, respectively.

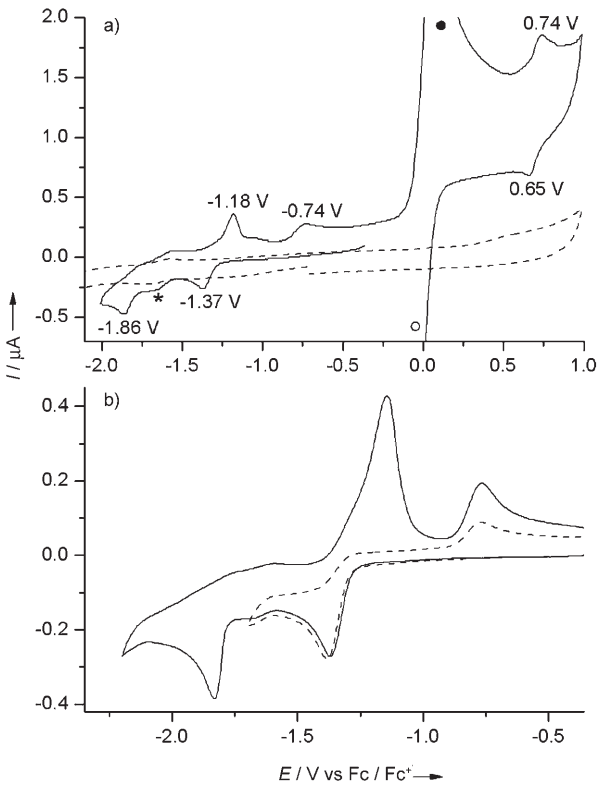

Figure 2. a) Cyclic voltammograms of $Dy_3N@C_{80}$(I) in $TBABF_4$/*o*-DCB with ferrocene (Fc) as the internal standard (——) and a blank $TBABF_4$/*o*-DCB electrolyte solution (-----). Scan rate: 100 mV s^{-1}. The open and filled circles mark the reduction and reoxidation peaks (off the scale) of ferrocene, respectively. The asterisk labels an unidentified reduction peak. The peak potentials are written above/below the peaks. b) Cathodic part of the cyclic voltammogram of $Dy_3N@C_{80}$(I) at 100 mV s^{-1} (——) as well as the first reduction step (-----).

as reference. The cyclic voltammogram of $Dy_3N@C_{80}$(I) exhibits quite a similar redox pattern to the recently reported $Tm_3N@C_{80}$(I)[18] and consists of two electrochemically irreversible reduction steps, as given in Figure 2b, and one reversible oxidation step. Also included in Figure 2b is the

first reduction step of the cyclic voltammogram of $Dy_3N@C_{80}$(I), clearly indicating the first reduction peak and the strongly shifted reoxidation peak of the species generated from the fullerene monoanion. Because of the evident electrochemical irreversibilities of the two reduction steps, it is important to identify the individual reduction steps and the correlated reoxidation steps so as to establish the redox-reaction mechanism.

To separate the reactions of the first and the second reduction steps, a cyclic voltammogram ending the back scan at a reoxidation potential of ≈ -0.92 V, which is a value in between those of the two reoxidation peaks, was measured and gave no significant change in the shape and intensity of the second reduction peak or its reoxidation peak (see Figure 3). Thus, the correlation of the reoxidation peak at

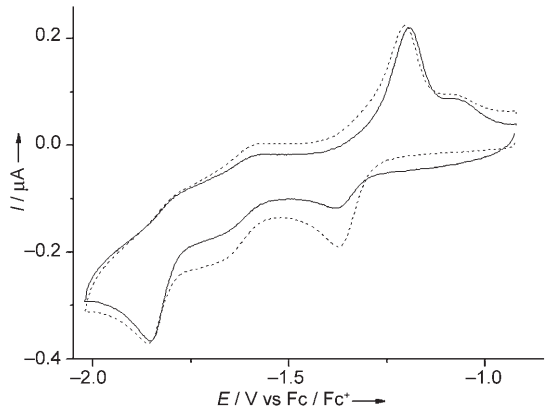

Figure 3. Cathodic part of the cyclic voltammogram of $Dy_3N@C_{80}$(I) using the back scan up to the reoxidization potential of −0.92 V for the 5th cycle (——) compared with the 1st cycle (-----). Scan rate: 50 mV s^{-1}.

−0.74 V with the first reduction peak at −1.37 V and the other anodic peak at −1.18 V with the second reduction peak (−1.86 V) is reasonable (see Figures 2 and 3). Moreover, no significant change in the shape and intensity of the peaks during multiple redox cycles was observed. For instance, the cyclic voltammogram in the potential range from −0.92 to −2.02 V during the fifth cycle (Figure 3) largely preserved the features of that obtained during the first cycle, except that the intensity of the first reduction peak decreased because the potential in the back scan was not high enough for full reoxidation to occur. Therefore, the redox reaction is clearly chemically reversible under the present conditions. Further confirmation of the chemical reversibility of the redox reactions was fulfilled by LD-TOF mass spectroscopic measurements performed with the sample solutions after the voltammetric measurements mentioned above, revealing that the peaks of the corresponding clusterfullerenes dominated the mass spectra in all cases (see also Figure 1) and no stable follow-up product of the clusterfullerenes was detected.

As a matter of fact, although the scan rate used in the present study (100 mV s^{-1}) was different from those reported in the literature (10 mV s^{-1}),[17,18] the first reduction peak potential ($E_{p,red(1)}$) of $Dy_3N@C_{80}$(I) (−1.37 V) was found to be close to that of $Tm_3N@C_{80}$(I) (−1.34 V)[18] but more negative than the formal potential of the first reduction step ($E_{1/2,red(1)}$) of $Sc_3N@C_{80}$(I) (−1.24 V).[17] Similarly, the second reduction peak potential of $Dy_3N@C_{80}$(I) (−1.86 V) was also found to be more negative than that of $Tm_3N@C_{80}$(I) (−1.78 V) and the $E_{1/2,red(2)}$ of $Sc_3N@C_{80}$(I) (−1.62 V). On the other hand, a fairly reversible oxidation step was observed for all cases. The formal potential of the oxidation step ($E_{1/2,ox(1)}$) of $Dy_3N@C_{80}$(I) is +0.70 V, which is quite close to those of $Tm_3N@C_{80}$(I) (+0.68 V) and $Sc_3N@C_{80}$(I) (+0.62 V).[17,18] Further detailed discussions on the redox-behavior difference is given below.

A large peak-to-peak separation in the first and second reduction steps (see Figures 2 and 3) can be understood by the following mechanism: A change in the molecular structure (geometry) accompanied by some energetical barrier and slow electron transfer might be possible.[27] Such a mechanism is illustrated in the double-square reaction scheme shown in Scheme 1, which will be discussed in detail below. On the other hand, another probable mechanism proposed for $Tm_3N@C_{80}$(I),[18] which is based on the assumption that the formation of a reaction product of the corresponding anion gives rise to the strongly shifted reoxidation peak, should be excluded according to the results of the above-mentioned LD-TOF mass-spectroscopic measurements.

Cyclic voltammogram of $Dy_3N@C_{80}$(I) at fast scan rates and the redox-reaction mechanism: It is important to state that scan rates commonly used in cyclic voltammetry (CV) (in the range from 5 mV s^{-1} to 1 V s^{-1}) do not significantly change the shape of the cyclic voltammogram of $Dy_3N@C_{80}$(I), as illustrated in Figure 4 (only the first reduction step is shown). The larger peak-to-peak separations at higher scan rates are caused by the uncompensated iR drop (potential drop due to solution resistance) in the electrochemical cell.

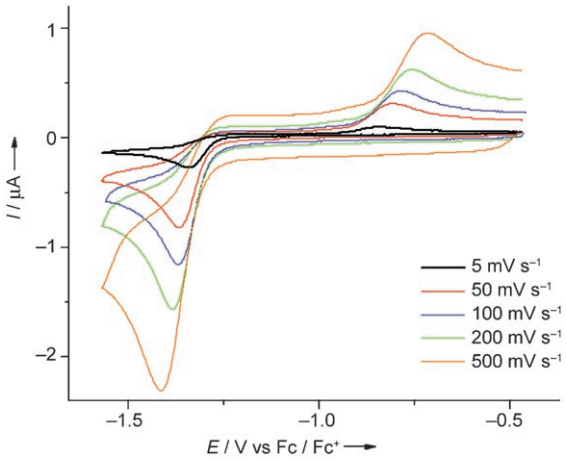

Figure 4. Cyclic voltammogram of the first reduction step of $Dy_3N@C_{80}$(I) at different scan rates (5–500 mV s^{-1}).

To fully understand the observed voltammetric behavior of $Dy_3N@C_{80}$(I), fast-scan CV with an even higher scan rate (up to 100 $V s^{-1}$) was measured and the results are presented in Figure 5. In the first reduction step (0–1 in Figure 5a–c), one electron is transferred to $Dy_3N@C_{80}(0)$ and its monoanion ($Dy_3N@C_{80}(1)$) is generated (see Scheme 1). This reduction step is followed by a fast (relative to the timescale of the experiment) structural rearrangement, that is, transformation of the geometric structure, resulting in the formation of a new stable species denoted as $Dy_3N@C_{80}(1')$. Due to the chemical reversibility of the redox reaction, as discussed above, the charge-induced structural rearrangement of monoanion $Dy_3N@C_{80}(1)$ is reversible and results from the change of the Dy_3N cluster (shape or position inside the cage), which is to be addressed in further studies.

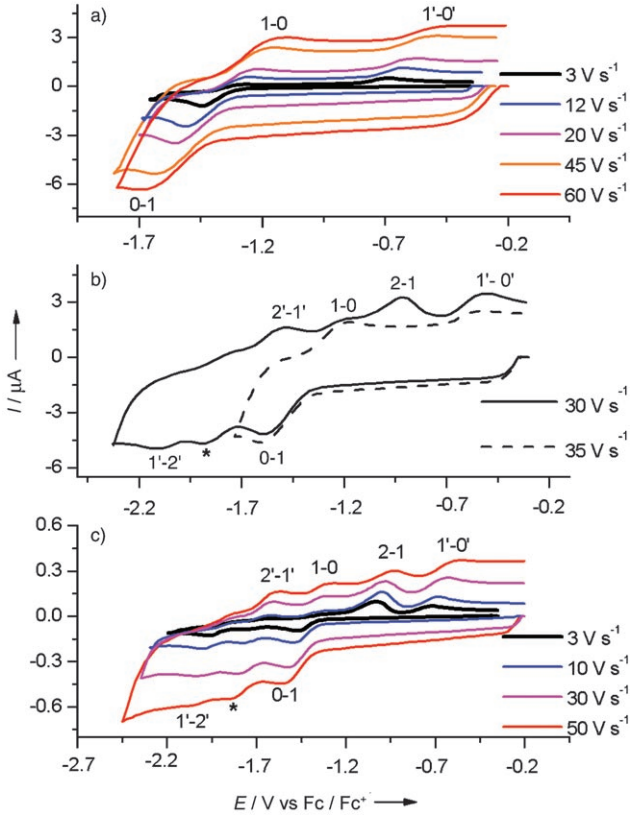

Figure 5. Fast-scan cyclic voltammograms of $Dy_3N@C_{80}$(I): a) The first reduction step at scan rates of 3–60 $V s^{-1}$. b) Cathodic part at a scan rate of 30 $V s^{-1}$ showing two reduction steps and the first reduction step at a scan rate of 35 $V s^{-1}$. c) Cathodic part at different scan rates (3–50 $V s^{-1}$). The labels of peaks are discussed in the text. The different current scale in (c) is due to the different electrode area of the Pt wire used as the working electrode.

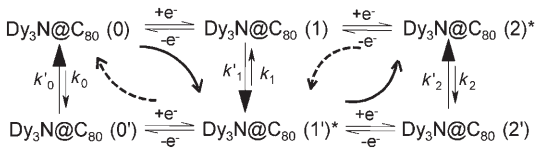

Scheme 1. Double-square reaction scheme of the electrochemical redox reaction of $Dy_3N@C_{80}$ (I). $Dy_3N@C_{80}$ (0), $Dy_3N@C_{80}$ (1), and $Dy_3N@C_{80}$ (2) represent the initial state of the molecule, the monoanion, and the dianion, respectively. Charge at the cage is not given. The stable species generated by the structural rearrangement are marked by asterisks. Black arrows with wider heads symbolize the preferable and fast structural rearrangements. The arc arrows show the main reaction pathways proposed (electrochemical–chemical–electrochemical–chemical (ECEC) mechanisms; forward scan = solid arrows, back scan = dashed arrows).

Furthermore, reoxidation of the $Dy_3N@C_{80}(1')$ species occurs at more positive potentials than that expected for reversible reoxidation of the monoanion and generates another species $Dy_3N@C_{80}(0')$. Such an oxidation peak is denoted as 1′–0′ in Figure 5a–c (also see Scheme 1). However, the $Dy_3N@C_{80}(0')$ form is unstable and consequently undergoes a fast transformation to the initial state $Dy_3N@C_{80}(0)$. A large peak-to-peak separation is therefore observed when using the conventional scan rates (see Figures 2 and 4). At scan rates higher than 3 $V s^{-1}$, an anodic peak (1–0 in Figure 5a–c) arising from the reoxidation of monoanion $Dy_3N@C_{80}(1)$ to neutral $Dy_3N@C_{80}(0)$ is already observable at the potential expected for reversible voltammetric behavior. However, the 1′–0′ peak is still present even at scan rates as high as 100 $V s^{-1}$, suggesting a much higher stability of $Dy_3N@C_{80}(1')$ relative to the monoanion $Dy_3N@C_{80}(1)$. Higher scan rates are hence needed to accomplish full electrochemical reversibility of the first reduction step. Based on these results, the timescale for the $Dy_3N@C_{80}(1)$–$Dy_3N@C_{80}(1')$ transformation falls into the range of tens of milliseconds.

Upon reduction at more negative potentials and scan rates of up to 3 $V s^{-1}$, a second reduction peak denoted as 1′–2′ in Figure 5b and c, which corresponds to the reduction of the monoanion $Dy_3N@C_{80}(1')$ to the dianion $Dy_3N@C_{80}(2')$, appears. The unstable product $Dy_3N@C_{80}(2')$ is then transformed into the stable $Dy_3N@C_{80}(2)$ form immediately. Its reoxidation peak is also shifted to a more positive potential similar to the first reduction step (see peak 2–1 in Figure 5b). Such a reoxidation reaction is preferentially followed by a structural rearrangement correlated with the $Dy_3N@C_{80}(1)$–$Dy_3N@C_{80}(1')$ pathway as discussed above, completing the second square cycle in the double-square reaction scheme (see Scheme 1). At scan rates higher than 3 $V s^{-1}$, direct reoxidation of the unstable $Dy_3N@C_{80}(2')$ to $Dy_3N@C_{80}(1')$ is already observed as a new anodic peak denoted as 2′–1′ appears (see Figure 5b and c). At such high scan rates, the relative intensity of the unidentified reduction peak between the 1′–2′ and 0–1 peaks (labeled with an asterisk) increases dramatically. Clearly, in this case the scan rate is high enough for the direct reduction of unstable monoanion $Dy_3N@C_{80}(1)$ to dianion $Dy_3N@C_{80}(2)$, and this is to be studied further.

Cyclic voltammogram of $Dy_3N@C_{80}$(II): The cyclic voltammogram of $Dy_3N@C_{80}$(II) is given in Figure 6 together with that of $Dy_3N@C_{80}$(I) for comparison. The difference in the current is due to the difference in the concentration of the sample used in the independent measurements. The cathodic part of the cyclic voltammogram is quite similar for both

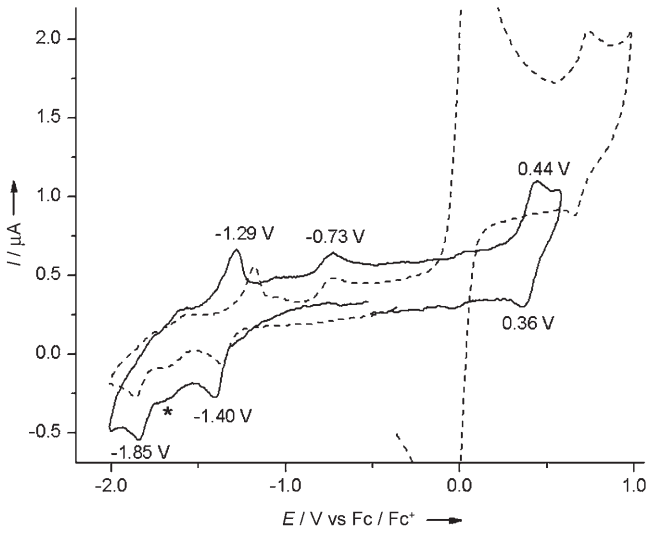

Figure 6. Cyclic voltammograms of $Dy_3N@C_{80}$(II) (——) and $Dy_3N@C_{80}$(I) (-----; copied from Figure 2) in $TBABF_4$/*o*-DCB. Scan rate: 100 mV s^{-1}. The asterisk labels an unidentified reduction peak. The peak potentials are written above/below the peaks.

isomers. The $E_{p,red(1)}$ of $Dy_3N@C_{80}$(II) is −1.40 V, exhibiting a slight negative shift compared with that of $Dy_3N@C_{80}$(I) (−1.37 V). In addition, the first reoxidation peak potential ($E_{p,reox(1)}$) and the second reduction peak potential ($E_{p,red(2)}$) are similar for both isomers, only the second reoxidation peak potential $E_{p,reox(2)}$ exhibits a difference (see Figure 6 and Table 1).

Table 1. Redox potentials and electrochemical energy gaps ($\Delta E_{gap,ec}$) of the studied $Dy_3N@C_{2n}$ clusterfullerenes.

	Redox potential (V vs Fc/Fc^+)			$\Delta E_{gap,ec}$ [V][c]
	$E_{p,red(1)}$[a]	$E_{p,red(2)}$[a]	$E_{1/2,ox(1)}$[b]	
$Dy_3N@C_{80}$(I)	−1.37	−1.86	0.70	2.07
$Dy_3N@C_{80}$(II)	−1.40	−1.85	0.41	1.81
$Dy_3N@C_{78}$(II)	−1.54	−1.93	0.47	2.01

[a] $E_{p,red}$: the reduction peak potential. [b] $E_{1/2,ox(1)}$: the formal oxidation potential of the first oxidation step. [c] $\Delta E_{gap,ec} = E_{1/2,ox(1)} - E_{p,red(1)}$.

The significant difference between the cyclic voltammograms of these two isomers of $Dy_3N@C_{80}$ appears in the anodic part. Although the reversibility of the oxidation step is largely attained for $Dy_3N@C_{80}$(II), its first formal oxidation potential ($E_{1/2,ox(1)}$) is 0.41 V, negatively shifted by 290 mV with respect to $Dy_3N@C_{80}$(I). In fact, a similar behavior for the two isomers of $Sc_3N@C_{80}$ with a potential difference of 270 mV was already demonstrated.[24] In addition to the empty fullerenes, some monometallofullerenes $M@C_{82}$ (M = La, Sc, Y, Pr) have also been reported to have a difference between the major and minor isomers of 143 mV for the first oxidation potential.[14,16]

Cyclic voltammogram of $Dy_3N@C_{78}$(II): $Dy_3N@C_{78}$(II) was preferably studied because of its much higher availability than that of the minor isomer $Dy_3N@C_{78}$(I).[25] The cyclic voltammogram of $Dy_3N@C_{78}$(II), exhibiting two electrochemically irreversible reduction steps and one reversible oxidation step (Figure 7), has in general a similar shape to

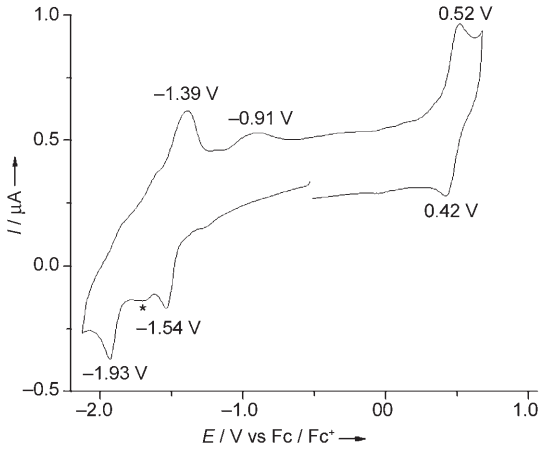

Figure 7. Cyclic voltammogram of $Dy_3N@C_{78}$(II) in $TBABF_4$/*o*-DCB. Scan rate: 100 mV s^{-1}. The asterisk labels an unidentified reduction peak. The peak potentials are written above/below the peaks.

those of $Dy_3N@C_{80}$(I) and $Dy_3N@C_{80}$(II) except that all of the reduction and reoxidation peaks in the cathodic part are negatively shifted. The formal potential of the oxidation peak ($E_{1/2,ox(1)}$) of $Dy_3N@C_{78}$(II) is 0.47 V, which is closer to that of $Dy_3N@C_{80}$(II). However, $Dy_3N@C_{78}$(II) resembles $Dy_3N@C_{80}$(I) more in terms of the electrochemical gap (see Table 1).

To address the effect of the endohedral structure on the electrochemical redox behavior of the C_{78} cage, the cyclic voltammogram of $Dy_3N@C_{78}$(II) was compared with both the empty C_{78} fullerene and the C_{78}-based metallofullerenes reported elsewhere (also see Table S1 in the Supporting Information).[22,23,28] For instance, the first and second reduction potentials of the C_{78} major isomer (C_{2v}) are −0.77 and −1.08 V, respectively, which coincide with those of the C_{78} minor isomer (D_3).[22] In this sense, the first and second reduction potentials of $Dy_3N@C_{78}$(II) are more negative than those of empty C_{78}, suggesting a lowered electron-accepting ability for the charged C_{78} cage owing to the encapsulation of the nitride cluster and consequently its charge transfer to the cage. On the other hand, the oxidation potentials of C_{2v}- and D_3-symmetric C_{78} isomers are 0.95 and 0.70 V, respectively,[22] which are both more positive than that of $Dy_3N@C_{78}$(II), confirming the stronger electron-donating ability of $Dy_3N@C_{78}$(II) relative to empty C_{78}. In fact, this is not the case for the C_{82} cage, for which the monometallofullerene $M@C_{82}$ (M = Y, La, Ce, Pr, Nd, Gd, Tb, Dy, Ho, Er, Lu, etc.) has not only a more positive reduction potential but also a more negative oxidation potential relative to the empty C_{82} cage.[1,11–16] It was found that the first reduction potential of $Dy_3N@C_{78}$(II) is much more negative than that of $La_2@C_{78}$ (D_{3h}),[28] a newly reported metallofullerene,

while their second reduction potentials are very close. However, the first oxidation potential of $Dy_3N@C_{78}$(II) is more positive than that of $La_2@C_{78}$ (D_{3h}). The first and second reduction potentials of $Dy_3N@C_{78}$(II) are also distinctly different from those of the monometallofullerene $Yb@C_{78}$.[23] Because the electrochemical redox behavior of endohedral fullerenes is dependent mainly on the nature of the fullerene cage,[1] such a distinct difference among these three C_{78}-based endohedral fullerenes suggests their significant difference lies in the symmetry of the fullerene cage and/or the charge transfer from the encaged species to the cage. Moreover, once the electrochemical data for minor isomer $Dy_3N@C_{78}$(I)[25] is available, it would be interesting to investigate whether these two isomers of $Dy_3N@C_{78}$ would follow the same behavior of reduction and oxidation potentials as revealed for the empty C_{78} isomers.

Effect of the encaged cluster on the electrochemical behavior of $M_3N@C_{80}$(I,II) (M = Dy, Sc, Tm): The molecular symmetries of $Dy_3N@C_{80}$(I) and $Dy_3N@C_{80}$(II) have been determined to be I_h and D_{5h}, respectively,[26] which are the same as their counterparts $Sc_3N@C_{80}$(I), $Tm_3N@C_{80}$(I), and $Sc_3N@C_{80}$(II).[17,18] This suggests a reason as to the similarity of their electronic structures, as further revealed in the present electrochemical study. However, $Dy_3N@C_{80}$(I) has a greater resemblance to $Tm_3N@C_{80}$(I) than $Sc_3N@C_{80}$(I) in terms of both the redox potentials and electrochemical gap. This result is fully consistent with the conclusion drawn from the results of chromatography, UV-visible-NIR, and FTIR studies.[26] The previous CV study of $Sc_3N@C_{80}$(I) and $Tm_3N@C_{80}$(I) demonstrated that both the redox potential and peak current ratio of reduction are strongly metal dependent and this is also the case for the oxidation.[17,18] Regardless of the proved contribution of the M_3N (M = Sc, Tm, Dy) wave function to the LUMO of $M_3N@C_{80}$(I) (M = Sc, Tm, Dy),[17,18] the significant contribution of the metal to the HOMO of $M_3N@C_{80}$(I) (M = Sc, Tm, Dy) was further confirmed on the basis of the systematical positive shifts of the first oxidation potential from 0.62 V in $Sc_3N@C_{80}$(I) through 0.68 V in $Tm_3N@C_{80}$(I) to 0.70 V in $Dy_3N@C_{80}$(I). This is understood by considering the difference in the charge transfer from the encaged cluster to the cage for $M_3N@C_{80}$(I) (M = Sc, Tm, Dy), which could be explained by the significant discrepancy in the effective valency of the metal atom, that is, 2.8, 2.9, and 2.4 for Dy, Tm, and Sc, respectively, as determined by high-energy spectroscopic studies.[18–21] As such, the same conclusion could also be drawn for $M_3N@C_{80}$(II) (M = Sc, Dy) by comparing the positive shifts of the first oxidation potential from 0.32 V in $Sc_3N@C_{80}$(II) to 0.41 V in $Dy_3N@C_{80}$(II) (see Table 1, and Table S1 in the Supporting Information).

Effect of the symmetry and size of the fullerene cage on the electrochemical behavior of $Dy_3N@C_{2n}$ ($2n$=78, 80): The electrochemical properties of the three $Dy_3N@C_{2n}$ clusterfullerenes studied in the present work appear to be dependent both on the isomeric structure and on the size of the fullerene cage. This can be understood by considering the difference in the electronic structures resulting from the different molecular symmetries. The negative shift of 290 mV for the first oxidation potential for $Dy_3N@C_{80}$(II) (D_{5h}) with respect to $Dy_3N@C_{80}$(I) (I_h) is in good agreement with the potential difference of 270 mV for the two isomers of $Sc_3N@C_{80}$,[24] clearly indicating that lowering the molecular symmetry of the clusterfullerene cage results in a dramatic negative shift of the first oxidation potential, that is, an increase in the electron-donating ability. With the correlation of the oxidation potential to the HOMO of the molecule,[17,18] this result suggests a prominent contribution of the cage symmetry to the HOMO of $M_3N@C_{80}$ (M = Sc, Dy) together with the metal contribution discussed above. On the other hand, the electron-accepting ability, deduced from the reduction behavior, does not seem to be as sensitive to the change of the molecular symmetry.

On reducing the cage size from $Dy_3N@C_{80}$ to $Dy_3N@C_{78}$, both the first and second reduction potentials are negatively shifted dramatically, suggesting a lowered electron-accepting ability for $Dy_3N@C_{78}$. Although the molecular symmetry of $Dy_3N@C_{78}$(II) has not yet been determined, the highest symmetry for the C_{78} cage is D_{3h},[30] which is much lower than those of $Dy_3N@C_{80}$(I) (I_h) and $Dy_3N@C_{80}$(II) (D_{5h}). This means that lowering the molecular symmetry by varying the cage size of the clusterfullerene from $Dy_3N@C_{80}$ to $Dy_3N@C_{78}$ might result in the dramatic shift of the reduction potential, implying a significant contribution of the cage symmetry to the LUMO of $Dy_3N@C_{2n}$. Based on these results, we may conclude that the cage symmetry (size) has a dramatic contribution to both the HOMO and the LUMO of the $Dy_3N@C_{2n}$ clusterfullerenes, which is to be further addressed and is underway in our group.

Electrochemical energy gap of the studied $Dy_3N@C_{2n}$ clusterfullerenes: The difference in electronic structure of the three $Dy_3N@C_{2n}$ clusterfullerenes studied in the present work was also revealed by the significant difference in their electrochemical energy gaps ($\Delta E_{gap,ec}$), which were obtained as the difference between the formal potential of the first oxidation step and the formal potential of the first reduction step as used in the literature.[17,18] In the present case of $Dy_3N@C_{2n}$, the formal potential of the first reduction step was not available because of the electrochemical irreversibility of the reduction steps as discussed above. The first reduction peak potential ($E_{p,red(1)}$) was therefore used as a practical substitution for an estimation. The $\Delta E_{gap,ec}$ values for $Dy_3N@C_{80}$(I), $Dy_3N@C_{80}$(II), and $Dy_3N@C_{78}$(II) were then calculated to be 2.07, 1.81, and 2.01 V, respectively (see Table 1). Interestingly, the difference of $\Delta E_{gap,ec}$, that is, $Dy_3N@C_{80}$(I) > $Dy_3N@C_{78}$(II) > $Dy_3N@C_{80}$(II), is consistent with the difference in the optical energy gap determined by UV-visible-NIR spectroscopy as given in Figure 8. In fact, based on the spectral onsets of 823, 929, and 933 nm, the band gaps of $Dy_3N@C_{80}$(I), $Dy_3N@C_{80}$(II), and $Dy_3N@C_{78}$(II) were calculated to be 1.51, 1.33, and 1.33 eV, respectively, indicating that these three $Dy_3N@C_{2n}$ cluster-

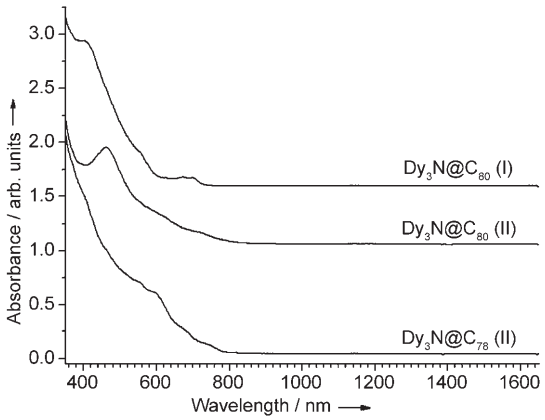

Figure 8. UV-visible-NIR spectra of $Dy_3N@C_{80}$(I), $Dy_3N@C_{80}$(II), and $Dy_3N@C_{78}$(II) samples dissolved in toluene.

fullerenes are all large-band-gap materials and electronically stable fullerenes.[25] While the energy gap could be used as an important indicator for evaluating the stability of a fullerene,[1,17,25] both the optical and electrochemical energy gaps appear to be important and should be evaluated together for the consistency of the result.

Conclusion

The electrochemistry of $Dy_3N@C_{80}$(I), $Dy_3N@C_{80}$(II), and $Dy_3N@C_{78}$(II) has been studied for the first time including their redox-reaction mechanism. The cyclic voltammogram of $Dy_3N@C_{80}$(I) (I_h) exhibits two electrochemically irreversible but chemically reversible reduction steps and one reversible oxidation step. In terms of both the redox potentials and electrochemical gap, a higher resemblance of $Dy_3N@C_{80}$(I) to $Tm_3N@C_{80}$(I) than to $Sc_3N@C_{80}$(I) was demonstrated. On the basis of a fast-scan CV study, a double-square reaction scheme was proposed to account for the observed redox-reaction behavior including the charge-induced reversible rearrangement of the $Dy_3N@C_{80}$(I) monoanion. The first oxidation potential of $Dy_3N@C_{80}$(II) (D_{5h}) has a negative shift of 290 mV relative to that of $Dy_3N@C_{80}$(I) (I_h), indicating that lowering the molecular symmetry of the clusterfullerene cage results in a pronounced increase in the electron-donating property, while the reduction potentials remain unchanged for these two isomers. As the first C_{78}-based clusterfullerene studied by electrochemistry, $Dy_3N@C_{78}$(II) demonstrates clear negative shifts of the first and second reduction potentials compared with those of $Dy_3N@C_{80}$(I and II), suggesting the former's lowered electron-accepting ability. The significant difference in the electrochemical HOMO–LUMO gaps of $Dy_3N@C_{80}$(I), $Dy_3N@C_{80}$(II), and $Dy_3N@C_{78}$(II) is consistent with their difference in optical energy gaps. In addition to the strong dependence of the electrochemical redox behavior and frontier molecular orbitals (HOMO and LUMO) on the cage symmetry, this study confirms the significant contribution of the metal to both the LUMOs and the HOMOs of $M_3N@C_{80}$(I) (M = Sc, Tm, Dy) and $M_3N@C_{80}$(II) (M = Sc, Dy). Further investigation into the origin of the charge-induced rearrangement of the $Dy_3N@C_{80}$(I) monoanion could be accomplished by using spectroscopic measurements to probe the change in the structure of the cluster.

Experimental Section

Tridysprosium nitride clusterfullerenes $Dy_3N@C_{80}$(I and II) and $Dy_3N@C_{78}$(II) were produced by a modified Krätschmer–Huffman DC-arc discharging method as reported elsewhere.[3,6,7,25,26] Laser desorption time-of-flight (LD-TOF) mass spectroscopic analyses running in both positive- and negative-ion modes (Biflex III, Bruker, Germany) were used to identify the $Dy_3N@C_{2n}$ clusterfullerenes and check the purity of the isolated clusterfullerenes. UV-visible-NIR spectra of the clusterfullerenes dissolved in toluene were recorded on a UV-Vis-NIR 3101-PC spectrometer (Shimadzu, Japan) using a quartz cell of 1 mm thickness.

Clusterfullerenes dissolved in toluene were dried, transported to a glove box (contents of oxygen and water were below 1 ppm), and immediately redissolved in *o*-dichlorobenzene (*o*-DCB, anhydrous, 99%, Aldrich). The concentration of the clusterfullerene in *o*-DCB ranged from 1×10^{-4} to 5×10^{-4} mol L^{-1}. The supporting electrolyte was tetrabutylammonium tetrafluoroborate ($TBABF_4$), which was dried under reduced pressure at 340 K for 24 h and stored in a glove box prior to use. The concentration of $TBABF_4$ in *o*-DCB ranged from 0.1 to 0.2 mol L^{-1}.

All CV experiments were performed with a PAR 273 potentiostat (EG&G, US) at room temperature. Inert conditions were achieved by bubbling nitrogen (N_2) before each measurement. A standard three-electrode arrangement of a platinum (Pt) wire as the working electrode, a platinum coil as the counter electrode, and a silver wire as the pseudoreference electrode was used. Ferrocene (Fc) was added as the internal standard for a final voltammetric cycle and all potentials were referred to an Fc/Fc^+ couple.

Acknowledgements

We cordially thank Mrs. H. Zöller, Ms. K. Leger and Mr. F. Ziegs for technical assistance. S.Y. and P.R. thank the Alexander von Humboldt (AvH) Foundation for financial support. The support of an IFW fellowship to M.Z. and SGA VEGA 1/3579/06 to P.R. are also acknowledged.

[1] H. Shinohara, *Rep. Prog. Phys.* **2000**, *63*, 843–892.
[2] *Endofullerenes: A New Family of Carbon Clusters* (Eds.: T. Akasaka, S. Nagase), Kluwer Academic Publishers, Dordrecht, **2002**.
[3] L. Dunsch, M. Krause, J. Noack, P. Georgi, *J. Phys. Chem. Solids* **2004**, *65*, 309–315.
[4] For a recent review, see: L. Dunsch, S. Yang, *Small*, submitted.
[5] S. Stevenson, G. Rice, T. Glass, K. Harich, F. Cromer, M. R. Jordan, J. Craft, E. Hajdu, R. Bible, M. M. Olmstead, K. Maitra, A. J. Fisher, A. L. Balch, H. C. Dorn, *Nature* **1999**, *401*, 55–57.
[6] L. Dunsch, P. Georgi, F. Ziegs, H. Zöller, German Patent DE 10301722 A1, **2003**.
[7] L. Dunsch, P. Georgi, M. Krause, C. R. Wang, *Synth. Met.* **2003**, *135*, 761–762.
[8] M. Krause, L. Dunsch, *Angew. Chem.* **2005**, *117*, 1581–1584; *Angew. Chem. Int. Ed.* **2005**, *44*, 1557–1560.
[9] L. J. Wilson, D. W. Cagle, T. P. Thrash, S. J. Kennel, S. Mirzadeh, J. M. Alford, G. J. Ehrhardt, *Coord. Chem. Rev.* **1999**, *192*, 199–207.
[10] E. B. Iezzi, F. Cromer, P. Stevenson, H. C. Dorn, *Synth. Met.* **2002**, *128*, 289–291.

[11] T. Akasaka, S. Nagase, K. Kobayashi, M. Walchli, K. Yamamoto, H. Funasaka, M. Kako, T. Hoshito, T. Erata, *Angew. Chem.* **1997**, *109*, 1716–1718; *Angew. Chem. Int. Ed. Engl.* **1997**, *36*, 1643–1645.
[12] W. Sato, K. Sueki, K. Kikuchi, K. Kobayashi, S. Suzuki, Y. Achiba, H. Nakahara, Y. Ohkuba, F. Ambe, K. Asai, *Phys. Rev. Lett.* **1998**, *80*, 133–136.
[13] T. Suzuki, Y. Maruyama, T. Kato, K. Kikuchi, Y. Achiba, *J. Am. Chem. Soc.* **1993**, *115*, 11006–11007.
[14] T. Suzuki, Y. Maruyama, T. Kato, K. Kikuchi, Y. Nakao, Y. Achiba, Y. Kobayashi, S. Nagese, *Angew. Chem.* **1995**, *107*, 1228–1230; *Angew. Chem. Int. Ed. Engl.* **1995**, *34*, 1094–1096.
[15] W. L. Wang, J. Q. Ding, S. H. Yang, X.-Y. Li in *Recent Advances in Chemistry and Physics of Fullerenes and Related Materials, Vol. 4* (Eds.: K. M. Kadish, R. S. Ruoff), Electrochemical Society, Pennington, **1997**, pp. 417–428.
[16] L. Z. Fan, S. F. Yang, S. H. Yang, *Chem. Eur. J.* **2003**, *9*, 5610–5617.
[17] M. Krause, L. Dunsch, *ChemPhysChem* **2004**, *5*, 1445–1449.
[18] M. Krause, X. J. Liu, J. Wong, T. Pichler, M. Knupfer, L. Dunsch, *J. Phys. Chem. A* **2005**, *109*, 7088–7093.
[19] L. Alvarez, T. Pichler, P. Georgi, T. Schwieger, H. Peisert, L. Dunsch, Z. Hu, M. Knupfer, J. Fink, P. Bressler, M. Mast, M. S. Golden, *Phys. Rev. B* **2002**, *66*, 035107.
[20] X. Liu, M. Krause, T. Pichler, L. Dunsch, M. Knupfer, *Phys. Rev. B* **2005**, *72*, 085407.
[21] H. Shiozawa, H. Rauf, T. Pichler, D. Grimm, X. Liu, M. Knupfer, M. Kalbac, S. Yang, L. Dunsch, B. Büchner, D. Batchelor, *Phys. Rev. B* **2005**, *72*, 195409.
[22] Y. Yang, F. Arias, L. Echegoyen, L. P. F. Chibante, S. Flanagan, A. Robertson, L. J. Wilson, *J. Am. Chem. Soc.* **1995**, *117*, 7801–7804.
[23] J. X. Xu, M. X. Li, Z. J. Shi, Z. N. Gu, *Chem. Eur. J.* **2006**, *12*, 562–567.
[24] B. Elliott, L. Yu, L. Echegoyen, *J. Am. Chem. Soc.* **2005**, *127*, 10885–10888.
[25] S. F. Yang, L. Dunsch, *J. Phys. Chem. B* **2005**, *109*, 12320–12328.
[26] S. F. Yang, L. Dunsch, *Chem. Eur. J.* **2006**, *12*, 413–419.
[27] P. Rapta, J. Kozisek, M. Breza, M. Gembicky, L. Dunsch, *J. Electroanal. Chem.* **2004**, *566*, 123–129.
[28] B. P. Cao, T. Wakahara, T. Tsuchiya, M. Kondo, Y. Maeda, G. M. A. Rahman, T. Akasaka, K. Kobayashi, S. Nagase, K. Yamamoto, *J. Am. Chem. Soc.* **2004**, *126*, 9164–9165.
[29] Y. Iiduka, O. Ikenaga, A. Sakuraba, T. Wakahara, T. Tsuchiya, Y. Maeda, T. Nakahodo, T. Akasaka, M. Kako, N. Mizorogi, S. Nagese, *J. Am. Chem. Soc.* **2005**, *127*, 9956–9957.
[30] P. W. Fowler, D. E. Manolopoulos, *An Atlas of Fullerenes*, Clarendon Press, Oxford, **1995**.

Received: December 15, 2005
Revised: February 6, 2006
Published online: July 25, 2006

